JGR Space Physics

RESEARCH ARTICLE
10.1029/2018JA026155

Rare Occurrence of Off-Equatorial Edge Initiating and Equatorward Surging Plasma Depletions Observed in OI 630-nm Imaging

Navin Parihar[1]

[1]Indian Institute of Geomagnetism, Navi Mumbai, India

Key Points:
- This is the first report of off-equatorial edge initiating and equatorward surging airglow depletions
- Unlike usual depletions in the Northern Hemisphere, observed depletions appeared like an *inverted tree fork junction* (somewhat similar to those reported from the Southern Hemisphere)

Correspondence to:
N. Parihar,
navindeparihar@gmail.com

Citation:
Parihar, N. (2019). Rare occurrence of off-equatorial edge initiating and equatorward surging plasma depletions observed in OI 630-nm imaging. *Journal of Geophysical Research: Space Physics*, *124*, 2887–2896. https://doi.org/10.1029/2018JA026155

Received 2 OCT 2018
Accepted 18 FEB 2019
Accepted article online 24 FEB 2019
Published online 2 APR 2019

Abstract Usual depletions in the Northern Hemisphere form a tree fork junction feature near the south (i.e., toward the equator) in all-sky airglow images, and its branches surge toward the north (i.e., poleward). We report in this paper unusual airglow depletions in OI 630.0-nm imaging over India that surged equatorward and formed an inverted tree fork junction feature on 3 January 2011. Airglow images showed faint signatures of medium-scale traveling ionospheric disturbances in the beginning that were east-west aligned and propagated toward equator. Within 06 to 18 min of its passing, turbulent structures were noted in the field of view, and two depleted patches appeared out of low airglow background over the off-equatorial edge. The apex height of the associated geomagnetic flux tubes varied from ~ 1,400 to 1,600 km. Later, these dark regions intensified and surged equatorward while drifting slowly toward west. While remaining almost steady, one of them further intensified and continued to surge equatorward. The second dark patch got linked up with another isolated depletion to form an elongated depleted feature. Next, the southern end of this attached feature surged equatorward. When two depletions were well formed, an inverted tree fork junction was noticeable. During this time, the equatorward motion of the equatorial ionization anomaly structure is also seen. To the best of our knowledge, this is the first imaging observation of an inverted tree fork junction feature and brings out the unknown facets of ionospheric irregularities.

Plain Language Summary Usual depletions form a tree fork junction feature near the equatorial edge in all-sky airglow images; its branches surge poleward. On 3 January 2011, unusual depletions were noted over India that surged equatorward and formed an inverted tree fork junction. We present an independent usual depletion event. Such an inverted feature has been not reported earlier to the best of our knowledge and brings out the unknown facets of ionospheric irregularities.

1. Introduction

Several interesting electrodynamical processes occur in the equatorial and low-latitude ionosphere, for example, equatorial electrojet, equatorial ionization anomaly (EIA), irregularities, equatorial midnight pressure bulge, and F_3 layer (Appleton, 1946; Batista et al., 1997; Kelley, 2009; Rastogi, 1959; Sreeja et al., 2010). Strong ionospheric current system (known as equatorial electrojet) exists in a thin latitude band of ~ ± 2° about the dip equator (Kobea et al., 1998; Rastogi, 1959). EIA refers to anomalous crests in the ionization distribution seen on both sides of magnetic equator with a trough in between them (Appleton, 1946; Rastogi, 1959). Characterized by irregular plasma distributions, irregularities are the ubiquitous feature of the equatorial and low-latitude ionosphere and have scale sizes ranging from few meters to several hundreds of kilometers. In the postsunset equatorial ionosphere, the height rise of the *F* layer, the suitable alignment of the solar terminator with the geomagnetic field lines, absence of the strong transequatorial wind, and necessary seed perturbations set up favorable conditions for initiation of the Rayleigh-Taylor instability (RTI) which then generates irregularities (Fejer & Kelley, 1980; Huba & Joyce, 2007; Hysell et al., 1990; Makela & Otsuka, 2012; Woodman, 2009; Zalesak & Ossakow, 1980).

Different ground-based instruments, for example, ionosondes, radars, scintillation experiments, and airglow imaging, have contributed to our understanding of ionospheric irregularities. Depending upon the measurement technique, terms like spread *F*, plumes, bubbles, depletions, and bite outs have been used to discuss them (Woodman, 2009). Irregularities are seen as spread echoes in frequencies or virtual heights in the ionograms and are termed spread *F* for historical reasons (Booker & Wells, 1938; Woodman, 2009). In the range-

time-intensity maps of the backscattered radar power, they appear as large-scale plasma depletions or bubbles or topside plumes (Rodrigues et al., 2012; Woodman & La Hoz, 1976). As an example, Hysell and Burcham (1998) studied large-scale plumes and their relationship with bottom-type irregularities using Jicamarca Unattended Long-term studies of the Ionosphere and Atmosphere radar observations. Under Study on Atmospheric Forcings and Responses campaign, Patra and Phanikumar (2009) discussed the behavior of plasma bubbles in 2008 (a period of low solar activity) using radar measurements over Gadanki, India. Scintillations of transionospheric radio signals have been used for studying scintillation-causing irregularities (Basu & Basu, 1981). Using spaced receiver scintillation observations, Bhattacharyya et al. (2002) studied the effects of geomagnetic activity on the dynamics of irregularities. Su et al. (2002) reported large-density dropout structures in the group of equatorial spread-*F* irregularities in the topside ionosphere using Republic of China Satellite measurements. Huba and Joyce (2007) termed such large-density dropouts as "bite-outs."

Irregularities are seen as quasi field-aligned intensity-depleted regions in all-sky airglow images and are referred to as bubbles or depletions (Mendillo & Baumgardner, 1982). Owing to their proven ability to cover large horizontal area, all-sky imaging observations have been immensely successful in studying the two-dimensional horizontal morphology of the equatorial plasma bubbles (EPBs) (Kelley et al., 2002, 2004; Makela et al., 2004; Makela & Kelley, 2003; Martinis et al., 2006, 2017; Martinis & Mendillo, 2007; Pimenta et al., 2003; Sahai et al., 2006, 2009; Shiokawa et al., 2004, 2015). Closer to the magnetic equator, airglow depletions associated with EPBs are seen as north-south (NS) aligned and wishbone-shaped depleted regions in OI 630.0-nm images (Fukushima et al., 2015; Mendillo & Baumgardner, 1982; Mukherjee et al., 1998; Sinha & Raizada, 2000; Taori et al., 2015; Taylor et al., 1997). Over off-equatorial stations, such depletions are seen as a complex structure that resembles a *tree fork* with its junction situated near the equatorial edge and the branches spread out toward the poles (Chapagain et al., 2012; Kelley et al., 2002; Liu et al., 2011; Makela et al., 2004; Martinis et al., 2006, 2017; Martinis & Mendillo, 2007; Otsuka et al., 2002; Shiokawa et al., 2004, 2015; Sun et al., 2016). In this report, we present for the first time airglow depletion structures that generated near the off-equatorial edge of imaging observations and extending in the direction of the magnetic equator. Unlike those usually observed in the Northern Hemisphere, airglow depletions appeared like an *inverted tree fork junction* (somewhat similar to those observed in the Southern Hemisphere). In Ranchi (23.3°N, 85.3°E, magnetic latitude ~ 19°N), India, an off-equatorial station, plasma depletion events were rare. Signatures of medium-scale traveling ionospheric disturbances (MSTIDs) were noted in imaging observations before the initiation of these unusual depletions. During their development (the rare structure), ionization anomaly was present over Ranchi station, India.

2. Instrumentation

Campaign-based nightglow observations were carried out at a temporary station Ranchi (23.3°N, 85.3°E, magnetic latitude ~ 19°N), India, in January 2011 using an all-sky imager. This f/4 optics-based imaging system comprises a Mamiya fisheye lens, a shutter unit, the six-filter wheel assembly, the reimaging optics, and a 512 × 512 pixels back-illuminated charge-coupled device as the detector. Parihar et al. (2017) have described this imaging system. At OI 630.0-nm heights (~ 250 km), useful horizontal coverage of this imager was about 1,800 km. We monitored OI 630.0-nm emission using a 2.2-nm narrow-band optical filter having ~ 77% transmittance. Nightglow emissions from the mesosphere-lower thermosphere region were also monitored. The imager recorded OI 630.0-nm images every 6 min with an exposure time of 60 s. On this night, the sky was clear and good imaging observations were possible for ~ 10 hr.

Using the technique discussed by Anderson et al. (2014), the images were flat-fielded to reduce inhomogeneous contribution at lower elevations due to van Rhijn effect and nonuniform sensitivity of the charge-coupled device detector at different pixels. Next, we created an averaged image using the image data for the night and subtracted this mean image from each image to enhance the airglow features. A step further, we performed contrast enhancement of the images. Using known astral positions and assuming OI 630.0-nm emission peak at 250 km, we carried out the geographic correction of the raw images. Several authors have discussed such geometrical calibration of the warped all-sky images (Garcia et al., 1997; Martinis et al., 2017). Our imager's field of view easily covers the footprints of geomagnetic field lines that map to apex altitudes from 300 to 1,500 km. Because of the lack of a standard calibration facility (comprising a tungsten

lamp), we could not perform absolute calibration of brightness in Rayleighs. Hence, the intensities are presented in arbitary units. Further, Ranchi being the temporary experimental site, other ionospheric measurements like ionosonde and total electron content were not available for in-depth analysis of this event. Solar and geomagnetic conditions were moderately quiet with Solar $F10.7$ cm radio flux = 91, $Kp < 2+$, $Ap = 5$, and Dst varying between −8 and 9 nT. We have utilized in situ measurements of ion densities at ~ 840 km altitude by Defense Meteorological Satellite Program (DMSP) flight F15 to support our study (Huang et al., 2001; http://cedar.openmadrigal.org).

3. Observations

3.1. Signatures of MSTIDs During 1242–1318 UT

Starting from the first image at 1242 Universal Time (UT) (Indian Standard Time, IST = UT + 0530), weak signatures of east-west (EW) oriented and southward propagating band structures were clear in the processed images till 1324–1330 UT. Using successive images, we constructed time-differenced (TD) images to enhance these faint features (Suzuki et al., 2009; Makela et al., 2011). Figures 1a–1c present a few illustrations of these TD images that reveal irregular and broken fronts (marked by front "f1," "f2," and "f3"). Further, to study their propagation and alignment, we generated keograms along the NS and EW directions using TD images (Shiokawa et al., 2015; shown in Figures 1d and 1e, respectively). Keograms clearly reveal the EW alignment and southward propagation of bands. We estimated their horizontal wavelength, phase speed and period to be ~ 254 ± 7 km, 190 ± 43 m/s, and 22 min, respectively. The propagation characteristics of these bands is somewhat similar to those of the MSTIDs reported earlier (Garcia et al., 2000; Shiokawa et al., 2003; Kubota et al., 2011; Fukushima et al., 2012; Shiokawa et al., 2013; Narayanan et al., 2014; Figueiredo et al., 2018). Table 1 summarizes the propagation characteristics of MSTIDs reported in few reports along with that noted in this present study. We have summed up the reports that are based on airglow observations, and this list is not extensive. Several investigators have reported MSTIDs that reached low latitudes (geomagnetic latitude 9–18°; Fukushima et al., 2012; Ogawa et al., 2009; Shiokawa et al., 2002). Makela et al. (2010) reported two events wherein MSTIDs reached very close to the magnetic equator. Hence, we interpret these observed features as MSTIDs that propagated to Ranchi.

3.2. Signatures of Retreat of EIA During 1348–1600 UT

Figure 2a presents OI 630.0-nm intensity (in arbitrary units) variation noted on this night. A rapid decrease of intensity marked the nocturnal variation during evening hours till 1348 UT because of the usual decrease of ionization (with the solar radiation being cut off). It is worth to mention here that keograms showed MSTIDs activity during this time. We found the intensity to increase from 1348 UT, form an elevated peak at about 1436 UT, and then decrease till 1600 UT. Parihar et al. (2018) have earlier discussed such a behavior of the intensity in the premidnight hours over a nearby location in 2009. Over Allahabad (25.5°N, 81.9°E, geomagnetic latitude ~ 16.30°N), India, Parihar et al. (2018) found a hump in intensity during 1530–1830 UT associated with the EIA motion. As other ground-based measurements were not available, we studied the electron densities measured by the DMSP satellite at ~ 847 km to address this issue. Figure 2b illustrates the DMSP electron densities over the Indian subcontinent, and Figure 2c displays the time information. At ~ 1400 UT, the DMSP measurements showed an increase in the electron densities below the 20–25°N geodetic latitudes. Possibly the equatorward motion of EIA during this time resulted in such behavior. Using the intensity variations over the zenith and a sample location over the south, we studied its equatorward motion and found the EIA to retreat equatorward at the speed of ~ 444 m/s.

3.3. Observations of Off-Equatorial Edge Initiating and Equatorward Surging Depletions

Figures 3a and 3b present two examples of off-equatorial edge initiating and equatorward surging airglow depletions seen in 630.0-nm images on 3 January 2011. Figure 3c is a typical example of usual airglow depletion seen over Ranchi (recorded at 1524 UT on 16 April 2012). We have shown the images in raw orientation as recorded by the imager and have added directional information next to them. Image time stamp information is in *hhmmss* format. As depletions were faint in raw gray scale images on 3 January, we have used color scale index (in arbitrary units) to bring out the features. Usual airglow depletions over Ranchi showed highly structured depleted regions that had the tree fork junction feature near the equatorward edge (i.e., over the south horizon), and its branches surged toward the pole (i.e., to the north; as shown in Figure 3c). Often bifurcations marked their eastward walls. In terms of apex height, their poleward development was

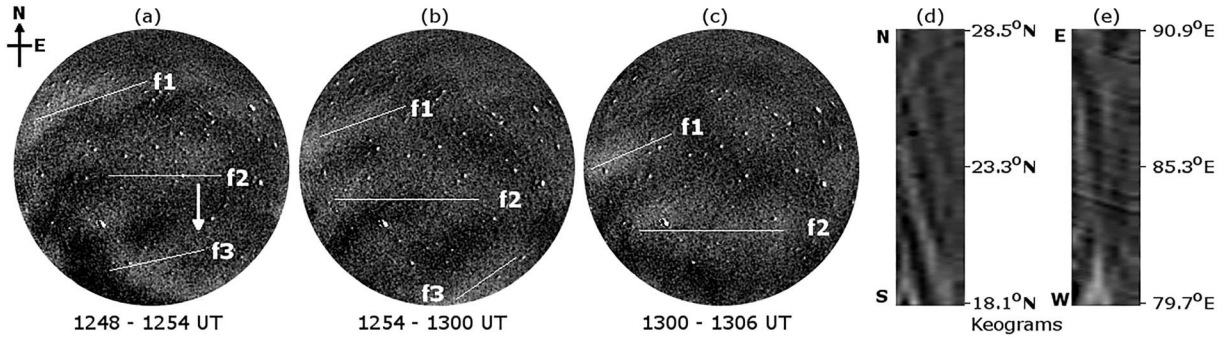

Figure 1. (a–c) Typical TD OI 630-nm images during 1242–1330 UT (IST = UT + 0530) on 3 January 2011 showing east-west aligned and southward propagating wave features over Ranchi. North-south and east-west keograms created from OI 630.0-nm TD images are shown in (d) and (e), respectively. Dark and bright striations indicate southward movement of wave trough and crest, respectively. TD = time-differenced.

between 400 and 1,000 km and seldom reached the extreme north horizon. In contrast, depleted features on this night appeared over the off-equatorial edge and stretched down toward the equatorial edge. Airglow images in Figures 3a and 3b reveal dark regions over the extreme north horizon. Apex height of these dark features lay between 1,400 and 1,600 km and have never being reported earlier from the Indian subcontinent. Further, these images show depleted regions hanging down toward the south (i.e., equatorward). Usual depletions were well marked against the background ionosphere (as seen in Figure 3c). In contrast, this event was fainter in nature. One of the possible reasons for this can be their appearance in the high-density plasma background associated with the EIA.

Figure 4 shows the sequence of images recorded during 1354–1448 UT that feature this event. Again, the image timestamp information is in hhmmss format. Being faint, depleted features near the edges during 1354–1418 UT were getting lost during geographic unwarping process. Hence, we have only presented flat-fielded, mean subtracted, and contrast enhanced images. During 1336–1400 UT, two depleted regions or dark oval patches appeared out over the north horizon in 28–29°N latitude regime. These dark patches map to apex heights of ~ 1,400–1,600 km over the geomagnetic equator and are more distinct around 1400–1406 UT. We mark two dark patches as DP1 and DP2 in OI 630.0-nm image at 1406 UT in Figure 4 for ease in description. Dark patch DP2 lay in close vicinity of the Pole Star (Polaris) (about its northeast), while DP1 appeared further toward the east and about 300 km from DP2. Dark patch DP2 was the first to emerge and almost followed the MSTIDs event with the images showing its faint signatures at ~ 1336 UT. Dark patch DP1 appeared about 12–18 min after the MSTIDs occurrence. As inferred from the geographically corrected images (not shown here), DP2 was tilted at an angle of ~ 18° to the west of DP1 during 1400–1406 UT. Later on, this tilt of two dark patches almost disappeared. As two dark regions intensified during 1406–1418 UT, they (especially DP1) showed unusual southward or equatorward surge and drifted

Table 1
Characteristics of MSTIDs Reported Earlier and That Observed in the Present Study

Reference	Airglow station	Horizontal wavelength (km)	Phase speed (m/s)	Observed period (min)
Garcia et al. (2000)	Arecibo (18.3°N, 66.75°W, geomagnetic latitude ~ 28.8°N), Puerto Rico	50–500	50–170	15–150
Shiokawa et al. (2003)	Rikubetsu (43.5°N, 143.8°E, geomagnetic latitude ~ 34.5°N) and Shigaraki (34.8°N, 136.1°E, geomagnetic latitude ~ 25.2°N), Japan	100–300	50–100	30–90
Kubota et al. (2011)	Poker Flat Research Range (65.1°N, 147.4°W, geomagnetic latitude ~ 65.62°N), Alaska	100–450	60–220	15–60
Fukushima et al. (2012)	Kototabang (0.2°S, 100.3°E, geomagnetic latitude ~ 10.6°S), Indonesia	790 ± 440	320 ± 170	42 ± 11
Shiokawa et al. (2013)	Tromsø (69.6°N, 19.2°E, geomagnetic latitude ~ 67.1°N), Norway Athabasca (54.7°N, 113.3°W geomagnetic latitude ~ 61.7°N), Canada	150–200	50–80	30–60
Narayanan et al. (2014)	Yonaguni (24.5°N, 123.0°E, geomagnetic latitude ~ 19.3°N), Japan	100–400	30–120	30–90
Figueiredo et al. (2018)	Cachoeira Paulista (22.4°S, 45.0°W, geomagnetic latitude ~ 13.6°S), Brazil	80–160	50–200	5–45
Present study	Ranchi (23.3°N, 85.3°E, geomagnetic latitude ~ 14.0°N), India	254 ± 7	190 ± 43	22

Note. Please note that this list is not extensive. MSTIDs = medium-scale traveling ionospheric disturbances

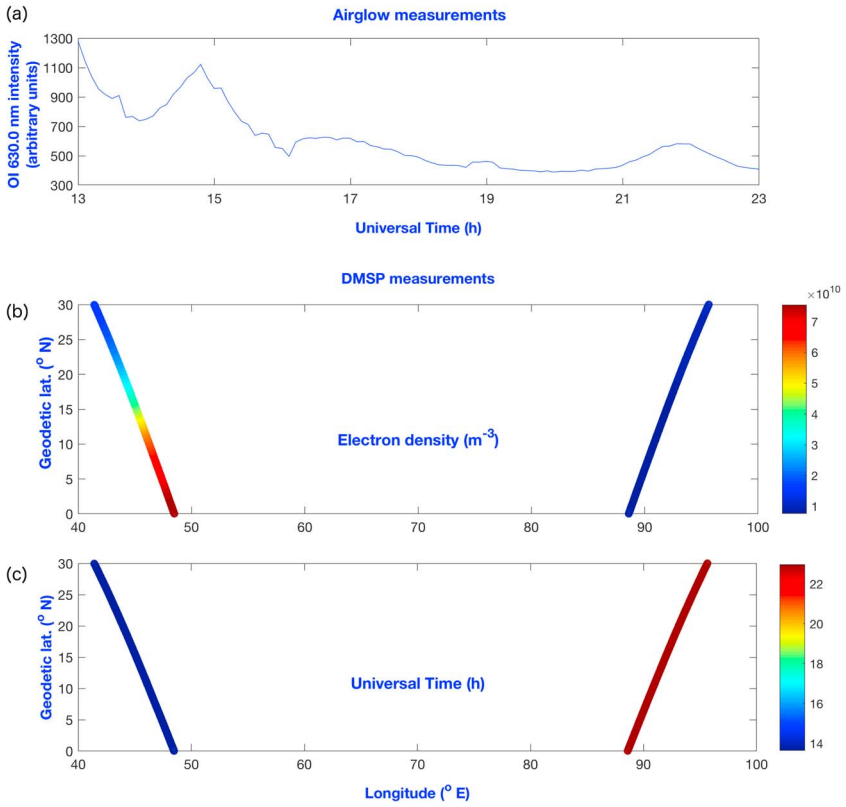

Figure 2. (a) Nocturnal variation of 630.0-nm intensity (in arbitrary units) on 3 January 2011. Defense Meteorological Satellite Program measurements of (b) the electron density at ~ 847 km over the Indian subcontinent and (c) corresponding Universal Time of measurements, respectively.

to the west with the speed of ~ 41–56 m/s. DP1 continued to intensify and surge equatorward till around 1442–1448 UT. However, DP2 showed some unusual behavior and got linked up with another depletion that was meanwhile evolving over its south.

Beginning ~ 1400 UT, OI 630-nm images showed a NS aligned isolated depletion next to Orion constellation and toward its east. We mark this isolated depletion by arc "a1" in the image at 1400 UT in Figure 4. Initially, this depletion was faint and geomagnetically aligned with DP1 during 1354–1400 UT. Later on, this depletion intensified, suffered a westward tilt, surged northward and aligned with DP2 at ~ 1418 UT. At ~ 1424 UT, this poleward surging depletion a1 got linked up with the equatorward surging DP2 over ~ 26°N, 88°E to form an elongated depleted feature. About this time, its NS extension was greater than 1,000 km.

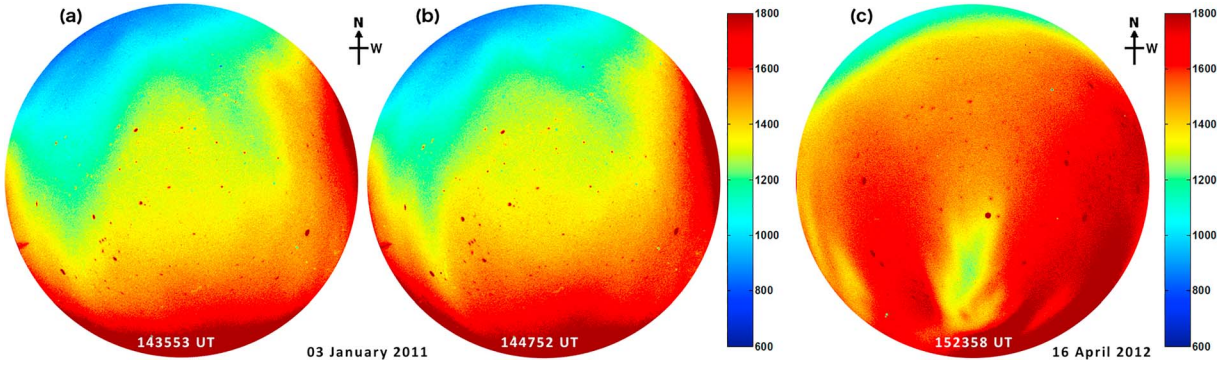

Figure 3. (a, b) Typical examples of off-equatorial edge initiating and equatorward surging depletions (appearing like *inverted tree fork junction depletions* in OI 630.0-nm imaging) on 3 January 2011 over Ranchi. (c) A typical example of airglow depletion usually seen over Ranchi (16 April 2012 at 1524 UT).

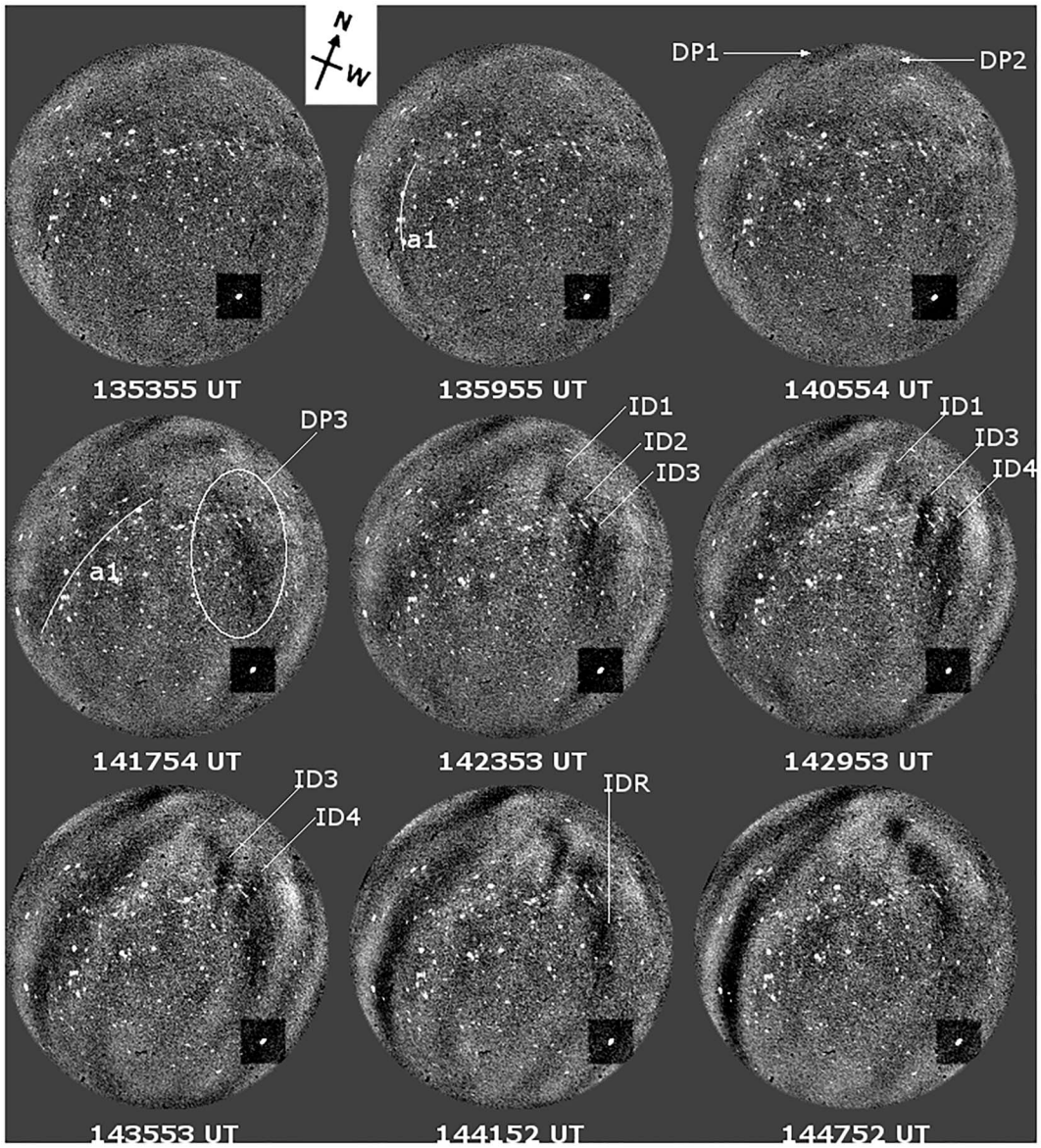

Figure 4. Sequence of OI 630.0-nm images recorded during 1354–1448 UT showing temporal evolution of different airglow depletions. Unusual *inverted tree fork junction type depletions* can be seen especially during 1429–1448 UT.

Next, this united feature surged equatorward and its walls sharpened (i.e., the gradients near its edges enhanced). During this time, DP1 remained almost stationary in terms of the zonal drift; however, DP2 showed an eastward motion. Around 1448 UT, their northern ends almost merged, and an inverted tree fork junction feature is evident (similar to those observed in the Southern Hemisphere). Figure 5a shows the corresponding geographically corrected (unwarped) image. Figure 5b presents the geometry of geomagnetic field lines over the 0–30° latitude range. When well-developed, the spacing between them was ~ 271 km at ~ 1448 UT over ~ 23°N. During the entire development, low airglow background existed over 28–29°N latitudes. Meanwhile, we found an increase in the background's intensity (because of ascent of the EIA over Ranchi). We also noticed few plasma blobs next to both DP1 and united DP2 during 1442–1448 UT.

Over the western sector of the field of view, a nonuniform region existed that hosted few isolated depletions. We have marked this region as DP3 in the image at 1418 UT in Figure 4 and named the isolated depletions as ID1, ID2, ID3, ID4, and IDR. ID1 and ID2 appeared as elongated dark regions, while ID3 and ID4 were seen as the inverted and elongated teardrop-shaped features. The apex height of these isolated depletions lay

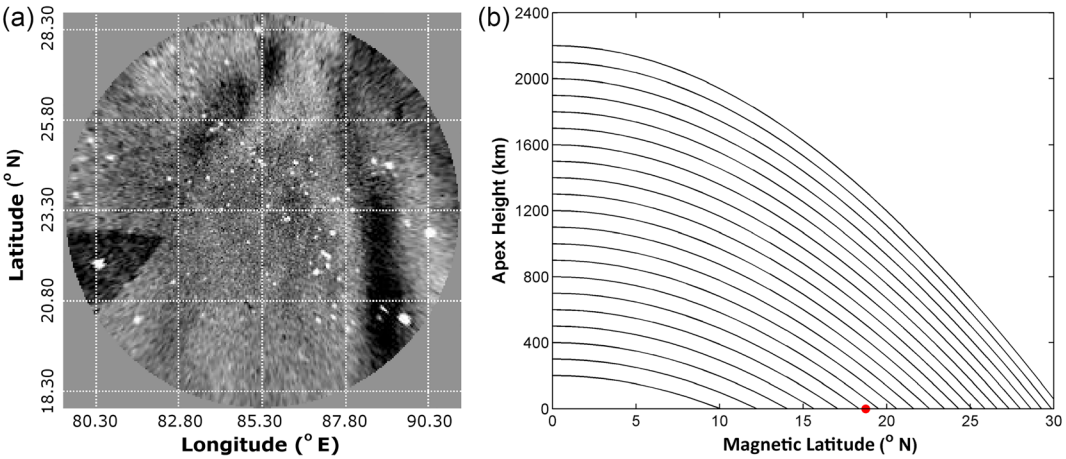

Figure 5. (a) Unwarped image at 1448 UT depicting *inverted tree-fork junction depletions*. (b) Geometry of geomagnetic field lines over 0–30° latitude range. Airglow observing station "Ranchi" is marked by red solid circle.

between 900 and 1,400 km, and these depletions drifted eastward with the speeds varying between 83 and 139 m/s. Few of these depletions subsequently merged to form a dark region near Polaris (apex height ~ 1,400 km) at ~ 1448 UT. Later on, these features disappeared within next 24–30 min.

4. Discussions

Often the generation of irregularities by RTI is confined within a few degrees of the magnetic equator (Fejer & Kelley, 1980; Fritts et al., 2009; Kelley, 2009; Woodman, 2009; Makela & Otsuka, 2012, and references therein). Ranchi being an off-equatorial station near the northern crest of EIA, such unusual airglow depletions observed under geomagnetic quiet conditions presents an interesting case. First, the images showed the signatures of MSTIDs propagating equatorward till around 1318 UT. Nonequatorial MSTIDs can trigger EPBs (Garcia et al., 2000; Krall et al., 2011; Miller et al., 2009; Taori et al., 2015). Soon after its passage, irregular turbulent regions formed in the field of view around 1324–1330 UT. Next, two dark patches, namely, DP1 and DP2, emerged over the off-equatorial edge out of low intensity background associated with the anomaly zone. Notably their separation (~ 300 km) almost matched the wavelength of MSTIDs, namely, 254 km. Dark patch DP1 intensified, drifted to west and surged toward equator. Likewise, dark patch DP2 built up, showed a westward drift, surged equatorward, and got linked up with another isolated depletion a1. Next, this united feature reversed its drift (from west to east) and surged toward the equator. When well-developed, DP1 and DP2 formed *unusual inverted tree fork junction feature* which is the usual feature of the imaging from the south of geomagnetic equator. About this time, their spacing (~ 271 km) quite equalled the wavelength of MSTIDs. During the time, the EIA (an enhanced plasma density feature) was impending Ranchi. Present observations thus make up a rare event involving the MSTIDs, the EIA, and associated airglow depletions.

Near-instantaneous appearance of dark patches after the MSTIDs passage suggests their possible role in triggering this unusual depletion event. Close matching between the dark patches/depletions spacing with the wavelength of the MSTIDs further supports this view. Probably the internal polarization electric field associated with the MSTIDs acted as the needed seed to trigger RTI that generated these depletions (Krall et al., 2011; Miller et al., 2009). Further, these dark patches appeared over a low airglow background in the northern extreme, that is, in a region uplifted from the rest of the field of view. The EW drift of airglow depletions is an indicator of the zonal motion of background plasma. First DP1 and DP2 were drifting toward west. During this time, depleted region a1 tilted to west, and later on, linked up with DP2. Next, DP1 remained almost stationary, while united depleted feature DP2 showed a reversal of drift from west to east. About this time, depletions ID1, ID2, ID3, and ID4 were drifting toward east. This illustrates that this event occurred under an abnormal zonal wind condition. Miller et al. (2009) have earlier reported the shear in drift introduced by MSTIDs. When DP1 and DP2 were well developed, their latitudinal extension was over 1,000 km. The northern end of DP1 and DP2 had the geomagnetic apex height between 1,400 and

1,600 km. Airglow depletions having such apex heights have never been reported from India to the best of our knowledge (Patra & Phanikumar, 2009, and references therein).

Kelley et al. (2000) have earlier reported an unusual event over Arecibo, Puerto Rico, wherein an airglow depletion surged poleward out of a well-developed equatorial anomaly. In their study, (i) there was an uplifted zone of low airglow, (ii) the drift was to west, and (iii) the meridional plasma drift was strong (much similar to the present study). In the same report, they presented the observations of a weak packet of high and low airglow patches. Authors found these patches to intensify in place, rotate toward the traveling ionospheric disturbance, and then reverse drift from southwest to northeast. Garcia et al. (2000) reported another poleward surging event triggered by MSTIDs. Authors found the depletions to develop from a dark region in a low airglow background and link up with another depletion. Garcia et al. (2000) and Kelley et al. (2000) pointed out toward the secondary role of $\mathbf{E} \times \mathbf{B}$ instability in their growth besides the primary Perkins instability.

5. Conclusions

For the first time, we report two depletions extending in the direction of the magnetic equator that later on formed an unusual inverted tree fork junction feature using all-sky airglow imaging over Ranchi (magnetic latitude ~ 19°N), India, on 3 January 2011. A serious limitation of this study is lack of other ionospheric data, for example, ionosonde and GPS total electron content measurements and would have thrown more light in its understanding. The salient features of this study are as follows:

1. First airglow images showed faint signatures of MSTIDs (λ ~ 254 km, υ ~ 190 m/s, and τ ~ 22 min) propagating equatorward during 1242–1330 UT. Soon after its passage, turbulent structures appeared in the field of view and two dark patches developed over the off-equatorial edge (apex heights ~ 1,400–1,600 km). Surprisingly their separation almost matched the MSTIDs wavelength.
2. Next, these dark patches intensified, surged equatorward, and drifted to the west. One of them continued to intensify, surge equatorward, and cease to drift toward west. Second dark patch surged a little toward the equator and linked up with another isolated depletion that was meanwhile emerging toward its south. Afterward, its walls and this unified depletion surged toward the equator.
3. When well developed, two depletions formed an inverted tree fork junction (a common feature observed in the imaging of depletions in the Southern Hemisphere). Also, their separation almost matched the wavelength of MSTIDs and their latitudinal extension was over 1,000 km. Such extended depletions are rare near the crest of EIA and have not been reported from an off-equatorial Indian station to the best of our knowledge.

Such equatorward surging airglow depletions have not been reported/discussed earlier and makes the present study a new line of research.

Acknowledgments
Funds for Airglow Research at Indian Institute of Geomagnetism are being provided by Department of Science and Technology (DST), Government of India, New Delhi. N. P. gratefully acknowledges award of (i) Junior Associateship, International Centre for Theoretical Physics, Trieste, Italy, and (ii) 2018 ISEE International Joint Research Award, Institute for Space-Earth Environmental Research (ISEE), Nagoya University, Japan. We gratefully acknowledge the receipt of DMSP data from Boston College, Institute for Scientific Research, Chestnut Hill, MA, USA (https://dmsp.bc.edu/ or http://cedar.openmadrigal.org). Imaging data are available upon request from the Indian Institute of Geomagnetism, India via the website (http://iigm.res.in/content/data-and-service-request-form).

References

Anderson, D. S., Makela, J. J., & Kanwar, U. (2014). Experimental validation of a technique to estimate vertical wavelength parameters from gravity wave perturbations on mesospheric airglows. *IEEE Transactions on Geoscience and Remote Sensing*, *52*(4), 1982–1990. https://doi.org/10.1109/TGRS.2013.2257176

Appleton, E. V. (1946). Two anomalies in the ionosphere. *Nature*, *157*(3995), 691. https://doi.org/10.1038/157691a0

Basu, S., & Basu, S. (1981). Equatorial scintillation—A review. *Journal of Atmospheric and Terrestrial Physics*, *43*(5–6), 473–489. https://doi.org/10.1016/0021-9169(81)90110-0

Batista, I. S., Sastri, J. H., deMedeiros, R. T., & Abdu, M. A. (1997). Nighttime thermospheric meridional winds at Cachoeira Paulista (23°S, 45°W): Evidence for effects of the equatorial midnight pressure bulge. *Journal of Geophysical Research*, *102*(A9), 20,059–20,062. https://doi.org/10.1029/97JA01387

Bhattacharyya, A., Basu, S., Groves, K. M., Valladares, C. E., & Sheehan, R. (2002). Effect of magnetic activity on the dynamics of equatorial *F* region irregularities. *Journal of Geophysical Research*, *107*(A12), 1489. https://doi.org/10.1029/2002JA009644

Booker, H. G., & Wells, H. W. (1938). Scattering of radio waves by the *F*-region of the ionosphere. *Terrestrial Magnetism and Atmospheric Electricity*, *43*(3), 249–256. https://doi.org/10.1029/TE043i003p00249

Chapagain, N. P., Taylor, M. J., Makela, J. J., & Duly, T. M. (2012). Equatorial plasma bubble zonal velocity using 630.0 nm airglow observations and plasma drift modeling over Ascension Island. *Journal of Geophysical Research*, *117*, A06316. https://doi.org/10.1029/2012JA01775

Fejer, B. G., & Kelley, M. C. (1980). Ionospheric irregularities. *Reviews of Geophysics*, *18*(2), 401–454. https://doi.org/10.1029/RG018i002p00401

Figueiredo, C. A. O. B., Takahashi, H., Wrasse, C. M., Otsuka, Y., Shiokawa, K., & Barros, D. (2018). Investigation of nighttime MSTIDS observed by optical thermosphere imagers at low latitudes: Morphology, propagation direction, and wind filtering. *Journal of Geophysical Research: Space Physics*, *123*, 7843–7857. https://doi.org/10.1029/2018JA025438

Fritts, D. C., Abdu, M. A., Batista, B. R., Batista, I. S., Batista, P. P., Buriti, R., et al. (2009). Overview and summary of the Spread *F* Experiment (SpreadFEx). *Annales Geophysicae*, *27*(5), 2141–2155. https://doi.org/10.5194/angeo-27-2141-2009

Fukushima, D., Shiokawa, K., Otsuka, Y., Nishioka, M., Kubota, M., Tsugawa, T., et al. (2015). Geomagnetically conjugate observation of plasma bubbles and thermospheric neutral winds at low latitudes. *Journal of Geophysical Research: Space Physics*, *120*, 2222–2231. https://doi.org/10.1002/2014JA020398

Fukushima, D., Shiokawa, K., Otsuka, Y., & Ogawa, T. (2012). Observation of equatorial nighttime medium-scale traveling ionospheric disturbances in 630-nm airglow images over 7 years. *Journal of Geophysical Research*, *117*, A10324. https://doi.org/10.1029/2012JA017758

Garcia, F. J., Kelley, M. C., Makela, J. J., Sultan, P. J., Pi, X., & Musman, S. (2000). Mesoscale structure of the midlatitude ionosphere during high geomagnetic activity: Airglow and GPS observations. *Journal of Geophysical Research*, *105*(A8), 18,417–18,427. https://doi.org/10.1029/1999JA000306

Garcia, F. J., Taylor, M. J., & Kelley, M. C. (1997). Two-dimensional spectra analysis of mesospheric airglow image data. *Applied Optics*, *36*(29), 7374–7385. https://doi.org/10.1364/AO.36.007374

Huang, C. Y., Burke, W. J., Machuzak, J. S., Gentile, L. C., & Sultan, P. J. (2001). DMSP observations of equatorial plasma bubbles in the topside ionosphere near solar maximum. *Journal of Geophysical Research*, *106*(A5), 8131–8142. https://doi.org/10.1029/2000JA000319

Huba, J. D., & Joyce, G. (2007). Equatorial spread *F* modeling: Multiple bifurcated structures, secondary instabilities, large density 'bite-outs,' and supersonic flows. *Geophysical Research Letters*, *34*, L07105. https://doi.org/10.1029/2006GL028519

Hysell, D. L., & Burcham, J. D. (1998). JULIA radar studies of equatorial spread *F*. *Journal of Geophysical Research*, *103*(A12), 29,155–29,167. https://doi.org/10.1029/98JA02655

Hysell, D. L., Kelley, M. C., Swartz, W. E., & Woodman, R. F. (1990). Seeding and layering of equatorial spread *F* by gravity waves. *Journal of Geophysical Research*, *95*(A10), 17,253–17,260. https://doi.org/10.1029/JA095iA10p17253

Kelley, M. C. (2009). *The Earth's ionosphere: Plasma physics and electrodynamics* (2nd ed.). Burlington, MA: Elsevier.

Kelley, M. C., Makela, J. J., Ledvina, B. M., & Kintner, P. M. (2002). Observations of equatorial spread-*F* from Haleakala, Hawaii. *Geophysical Research Letters*, *29*(20), 2003. https://doi.org/10.1029/2002GL015509

Kelley, M. C., Makela, J. J., Swartz, W. E., Collins, S. C., Thonnard, S., Aponte, N., & Tepley, C. A. (2000). Caribbean ionosphere campaign, year one: Airglow and plasma observations during two intense mid-latitude spread-*F* events. *Geophysical Research Letters*, *27*(18), 2825–2828. https://doi.org/10.1029/2000GL000022

Kelley, M. C., Swartz, W. E., & Makela, J. J. (2004). Mid-latitude ionospheric fluctuation spectra due to secondary $E \times B$ instabilities. *Journal of Atmospheric and Solar - Terrestrial Physics*, *66*(17), 1559–1565. https://doi.org/10.1016/j.jastp.2004.07.004

Kobea, A. T., Amory-Mazaudier, C., Do, J. M., Lühr, H., Houngninou, E., Vassal, J., et al. (1998). Equatorial electrojet as part of the global circuit: A case-study from the IEEY. *Annales Geophysicae*, *16*(6), 698–710. https://doi.org/10.1007/s00585-998-0698-1

Krall, J., Huba, J. D., Ossakow, S. L., Joyce, G., Makela, J. J., Miller, E. S., & Kelley, M. C. (2011). Modeling of equatorial plasma bubbles triggered by nonequatorial traveling ionospheric disturbances. *Geophysical Research Letters*, *38*, L08103. https://doi.org/10.1029/2011GL046890

Kubota, M., Conde, M., Ishii, M., Murayama, Y., & Jin, H. (2011). Characteristics of nighttime medium-scale traveling ionospheric disturbances observed over Alaska. *Journal of Geophysical Research*, *116*, A05307. https://doi.org/10.1029/2010JA016212

Liu, Y. J., Rajesh, P. K., Lee, I. T., & Chow, T. C. (2011). Airglow observations over the equatorial ionization anomaly zone in Taiwan. *Annales Geophysicae*, *29*(5), 749–757. https://doi.org/10.5194/angeo-29-749-2011

Makela, J. J., & Kelley, M. C. (2003). Field-aligned 777.4-nm composite airglow images of equatorial plasma depletions. *Geophysical Research Letters*, *30*(8), 1442. https://doi.org/10.1029/2003GL017106

Makela, J. J., Ledvina, B. M., Kelley, M. C., & Kintner, P. M. (2004). Analysis of the seasonal variations of equatorial plasma bubble occurrence observed from Haleakala, Hawaii. *Annales Geophysicae*, *22*(9), 3109–3121. https://doi.org/10.5194/angeo-22-3109-2004

Makela, J. J., Lognonné, P., Hébert, H., Gehrels, T., Rolland, L., Allgeyer, S., et al. (2011). Imaging and modeling the ionospheric airglow response over Hawaii to the tsunami generated by the Tohoku earthquake of 11 March 2011. *Geophysical Research Letters*, *38*, L00G02. https://doi.org/10.1029/2011GL047860

Makela, J. J., Miller, E. S., & Talaat, E. R. (2010). Nighttime medium-scale traveling ionospheric disturbances at low geomagnetic latitudes. *Geophysical Research Letters*, *37*, L24104. https://doi.org/10.1029/2010GL045922

Makela, J. J., & Otsuka, Y. (2012). Overview of nighttime ionospheric instabilities at low- and mid-latitudes: Coupling aspects resulting in structuring at the mesoscale. *Space Science Reviews*, *168*(1–4), 419–440. https://doi.org/10.1007/s11214-011-9816-6

Martinis, C., Baumgardner, J., Smith, S. M., Colerico, M., & Mendillo, M. (2006). Imaging science at El Leoncito, Argentina. *Annales Geophysicae*, *24*(5), 1375–1385. https://doi.org/10.5194/angeo-24-1375-2006

Martinis, C., Baumgardner, J., Wroten, J., & Mendillo, M. (2017). All-sky-imaging capabilities for ionospheric space weather research using geomagnetic conjugate point observing sites. *Advances in Space Research*, *61*(7), 1636–1651. https://doi.org/10.1016/j.asr.2017.07.021

Martinis, C., & Mendillo, M. (2007). Equatorial spread *F*-related airglow depletions at Arecibo and conjugate observations. *Journal of Geophysical Research*, *112*, A10310. https://doi.org/10.1029/2007JA012403

Mendillo, M., & Baumgardner, J. (1982). Airglow characteristics of equatorial plasma depletions. *Journal of Geophysical Research*, *87*(A9), 7641–7652. https://doi.org/10.1029/JA087iA09p07641

Miller, E. S., Makela, J. J., & Kelley, M. C. (2009). Seeding of equatorial plasma depletions by polarization electric fields from middle latitudes: Experimental evidence. *Geophysical Research Letters*, *36*, L18105. https://doi.org/10.1029/2009GL039695

Mukherjee, G. K., Carlo, L., Mahajan, S. H., & Patil, P. T. (1998). First results of all-sky imaging from India. *Earth, Planets and Space*, *50*(2), 119–127. https://doi.org/10.1186/BF03352093

Narayanan, V. L., Shiokawa, K., Otsuka, Y., & Saito, S. (2014). Airglow observations of nighttime medium-scale traveling ionospheric disturbances from Yonaguni: Statistical characteristics and low-latitude limit. *Journal of Geophysical Research: Space Physics*, *119*, 9268–9282. https://doi.org/10.1002/2014JA020368

Ogawa, T., Otsuka, Y., Shiokawa, K., Tsugawa, T., Saito, A., Hoshinoo, K., et al. (2009). Medium-scale traveling ionospheric disturbances and plasma bubbles observed by an all-sky airglow imager at Yonaguni, Japan. *Terrestrial, Atmospheric and Oceanic Sciences*, *20*(1), 287–295. https://doi.org/10.3319/TAO.2007.12.06.02(F3C

Otsuka, Y., Shiokawa, K., Ogawa, T., & Wilkinson, P. (2002). Geomagnetic conjugate observations of equatorial airglow depletions. *Geophysical Research Letters*, *29*(15), 1753. https://doi.org/10.1029/2002GL015347

Parihar, N., Radicella, S. M., Nava, B., Migoya-Orue, Y. O., Tiwari, P., & Singh, R. (2018). An investigation of the ionospheric *F* region near the EIA crest in India using OI 777.4 and 630.0 nm nightglow observations. *Annales Geophysicae*, *36*(3), 809–823. https://doi.org/10.5194/angeo-36-809-2018

Parihar, N., Singh, D., & Gurubaran, S. (2017). A comparison of ground-based hydroxyl airglow temperatures with SABER/TIMED measurements over 23°N, India. *Annales Geophysicae*, *35*(3), 353–363. https://doi.org/10.5194/angeo-35-353-2017

Patra, A. K., & Phanikumar, D. V. (2009). Intriguing aspects of *F*-region plasma irregularities revealed by the Gadanki radar observations during the SAFAR campaign. *Annales Geophysicae*, *27*(10), 3781–3790. https://doi.org/10.5194/angeo-27-3781-2009

Pimenta, A. A., Fagundes, P. R., Sahai, Y., Bittencourt, J. A., & Abalde, J. R. (2003). Equatorial *F*-region plasma depletion drifts: Latitudinal and seasonal variations. *Annales Geophysicae*, *21*(12), 2315–2322. https://doi.org/10.5194/angeo-21-2315-2003

Rastogi, R. G. (1959). The diurnal development of the anomalous equatorial belt in the F_2 region of the ionosphere. *Journal of Geophysical Research*, *64*(7), 727–732. https://doi.org/10.1029/JZ064i007p00727

Rodrigues, F. S., Moraes, A. O., & dePaula, E. R. (2012). Imaging equatorial spread *F* irregularities with the São Luís coherent backscatter radar interferometer. *Radio Science*, *47*, RS0L03. https://doi.org/10.1029/2011RS004929

Sahai, Y., Abalde, J. R., Fagundes, P. R., Pillat, V. G., & Bittencourt, J. A. (2006). First observations of detached equatorial ionospheric plasma depletions using OI 630.0 nm and OI 777.4 nm emissions nightglow imaging. *Geophysical Research Letters*, *33*, L11104. https://doi.org/10.1029/2005GL025262

Sahai, Y., Becker-Guedes, F., Fagundes, P. R., de Abreu, A. J., de Jesus, R., Pillat, V. G., et al. (2009). Observations of the *F*-region ionospheric irregularities in the South American sector during the October 2003 "Halloween storms". *Annales Geophysicae*, *27*(12), 4463–4477. https://doi.org/10.5194/angeo-27-4463-2009

Shiokawa, K., Ihara, C., Otsuka, Y., & Ogawa, T. (2003). Statistical study of nighttime medium-scale traveling ionospheric disturbances using mid-latitude airglow images. *Journal of Geophysical Research*, *108*(A1), 1052. https://doi.org/10.1029/2002JA009491

Shiokawa, K., Otsuka, Y., Ejiri, M. K., Sahai, Y., Kadota, T., Ihara, C., et al. (2002). Imaging observations of the equatorward limit of midlatitude traveling ionospheric disturbances. *Earth, Planets and Space*, *54*(1), 57–62, https://doi.org/10.1186/BF03352421

Shiokawa, K., Mori, M., Otsuka, Y., Oyama, S., Nozawa, S., Suzuki, S., & Connors, M. (2013). Observation of nighttime medium-scale travelling ionospheric disturbances by two 630-nm airglow imagers near the auroral zone. *Journal Atmospheric Solar-Terrestrial Physics,*, *103*, 184–194. https://doi.org/10.1016/j.jastp.2013.03.024

Shiokawa, K., Otsuka, Y., Lynn, K. J. W., Wilkinson, P., & Tsugawa, T. (2015). Airglow-imaging observation of plasma bubble disappearance at geomagnetically conjugate points. *Earth, Planets and Space*, *67*(1). https://doi.org/10.1186/s40623-015-0202-6

Shiokawa, K., Otsuka, Y., Ogawa, T., & Wilkinson, P. (2004). Time evolution of high-altitude plasma bubbles imaged at geomagnetic conjugate points. *Annales Geophysicae*, *22*(9), 3137–3143. https://doi.org/10.5194/angeo-22-3137-2004

Sinha, H. S. S., & Raizada, S. (2000). Some new features of ionospheric plasma depletions over the Indian zone using all sky optical imaging. *Earth, Planets and Space*, *52*(8), 549–559. https://doi.org/10.1186/BF03351662

Sreeja, V., Ravindran, S., & Pant, T. K. (2010). Features of the F_3 layer occurrence over the equatorial location of Trivandrum. *Annales Geophysicae*, *28*(9), 1741–1747, https://doi.org/10.5194/angeo-28-1741-2010

Su, S.-Y., Yeh, H. C., Chao, C. K., & Heelis, R. A. (2002). Observation of a large density dropout across the magnetic field at 600 km altitude during the 6–7 April 2000 magnetic storm. *Journal of Geophysical Research*, *107*(A11), 1404. https://doi.org/10.1029/2001JA07552

Sun, L., Xu, J., Wang, W., Yuan, W., Li, Q., & Jiang, C. (2016). A statistical analysis of equatorial plasma bubble structures based on an all-sky airglow imager network in China. *Journal of Geophysical Research: Space Physics*, *121*, 11,495–11,517. https://doi.org/10.1002/2016JA022950

Suzuki, S., Shiokawa, K., Liu, A. Z., Otsuka, Y., Ogawa, T., & Nakamura, T. (2009). Characteristics of equatorial gravity waves derived from mesospheric airglow imaging observations. *Annales Geophysicae*, *27*(4), 1625–1629. https://doi.org/10.5194/angeo-27-1625-2009

Taori, A., Parihar, N., Ghodpage, R., Dashora, N., Sripathi, S., Kherani, E. A., & Patil, P. T. (2015). Probing the possible trigger mechanisms of an equatorial plasma bubble event based on multistation optical data. *Journal of Geophysical Research: Space Physics*, *120*, 8835–8847. https://doi.org/10.1002/2015JA021541

Taylor, M. J., Eccles, J. V., LaBelle, J., & Sobral, J. H. A. (1997). High resolution OI (630 nm) image measurements of *F*-region depletion drifts during the Guara campaign. *Geophysical Research Letters*, *24*(13), 1699–1702. https://doi.org/10.1029/97GL01207

Woodman, R. F. (2009). Spread *F*—An old equatorial aeronomy problem finally resolved? *Annales Geophysicae*, *27*(5), 1915–1934. https://doi.org/10.5194/angeo-27-1915-2009

Woodman, R. F., & La Hoz, C. (1976). Radar observations of *F* region equatorial irregularities. *Journal of Geophysical Research*, *81*(31), 5447–5466. https://doi.org/10.1029/JA081i031p05447

Zalesak, S., & Ossakow, S. (1980). Nonlinear equatorial spread *F*: Spatially large bubbles resulting from large horizontal scale initial perturbations. *Journal of Geophysical Research*, *85*(A5), 2131–2142. https://doi.org/10.1029/JA085iA05p02131